How to cite this article: Karimi N, Khorashadizadeh M, Hanafi-Bojd MY, Alemzadeh E. Cefazolin-Loaded Double-Shelled Hollow Mesoporous Silica Nanoparticles /Polycaprolactone Nanofiber Composites: A Delivery Vehicle for Regenerative Purposes. Advanced Pharmaceutical Bulletin, doi: 10.34172/apb.2023.032

# Cefazolin-Loaded Double-Shelled Hollow Mesoporous Silica Nanoparticles /Polycaprolactone Nanofiber Composites: A Delivery Vehicle for Regenerative Purposes

Negar Karimi[1], Mohsen Khorashadizadeh[1], Mohammad Yahya Hanafi-Bojd[2, 3], Esmat Alemzadeh[1, 2]*

[1] Department of Medical Biotechnology, Faculty of Medicine, Birjand University of Medical Science, Birjand, Iran.
[2] Cellular and Molecular Research Center, Birjand University of Medical Sciences, Birjand, Iran.
[3]Nanomedicine Department, Faculty of Medicine, Birjand University of Medical Science, Birjand, Iran.

***Corresponding author:** Esmat Alemzadeh, E-mails: e.alemzadeh@bums.ac.ir; esmat.alemzadeh@gmail.com

Submitted: 10 July 2021
Revised: 31 January 2022
Accepted: 05 April 2022
ePublished: 05 April 2022

Negar Karimi : **https://orcid.org/0000-0002-3385-8279**
Esmat Alemzadeh: https://orcid.org/0000-0001-5287-4760

## Abstract

***Purpose*:** As important challenges in burn injuries, infections often lead to delayed and incomplete healing. Wound infections with antimicrobial-resistant bacteria are other challenges in the management of wounds. Hence, it can be critical to synthesize scaffolds that are highly potential for loading and delivering antibiotics over long periods.

***Methods*:** Double-shelled hollow mesoporous silica nanoparticles (DSH-MSNs) were synthesized and loaded with cefazolin. Cefazolin-loaded DSH-MSNs (Cef*DSH-MSNs) were incorporated into polycaprolactone (PCL) to prepare a nanofiber-mediated drug release system. Their biological properties were assessed through antibacterial activity, cell viability, and qRT-PCR. The morphology and physicochemical properties of the nanoparticles and nanofibers were also characterized.

***Results*:** The double-shelled hollow structure of DSH-MSNs demonstrated a high loading capacity of cefazolin (51%). According to *in vitro* findings, the Cef*DSH-MSNs embedded in polycaprolactone nanofibers (Cef*DSH-MSNs/PCL) provided a slow release for cefazolin. The release of cefazolin from Cef*DSH-MSNs/PCL nanofibers inhibited the growth of *Staphylococcus aureus*. The high viability rate of human adipose-derived stem cells (hADSCs) in contact with PCL and DSH-MSNs/PCL was indicative of the biocompatibility of nanofibers. Moreover, gene expression results confirmed changes in keratinocyte-related differentiation

genes in hADSCs cultured on the DSH-MSNs/PCL nanofibers with the up-regulation of involucrin.

***Conclusion*:** The high drug-loading capacity of DSH-MSNs presents these nanoparticles as suitable vehicles for drug delivery. In addition, the use of Cef*DSH-MSNs/PCL can be an effective strategy for regenerative purposes.

## Introduction

Today, chronic wounds are considered an emerging epidemic and have created serious clinical challenges for patients. A significant problem with chronic wounds is microbial biofilm formation, which delays wound healing.[1-3] Although the use of antibiotics has significantly reduced the risk of infections in patients, the widespread use of these drugs has increased the number of drug-resistant bacteria.[4] Hence, it would be a top priority to discover novel methods for inhibiting bacteria.[1]

Nanotechnology can help develop therapeutic strategies by designing drug delivery systems.[5-7] Advantages of drug delivery systems include improved hydrophobic drug solubility, increased drug half-life, prolonged systemic turnover, a slow release, reduced drug dosage, and targeted delivery of drug compounds. These characteristics overcome the limitations of traditional therapeutic approaches.[8,9] Among various delivery vehicles, mesoporous silica nanoparticles (MSNs) have gained much popularity in recent decades. Features such as high biocompatibility, high surface area, optimized mesoporous structure, and the ability to target and control drug release have proposed MSNs as promising materials for drug delivery.[10,11] Electrospinning is another promising technique that plays a vital role in drug delivery.[12,13] High encapsulation capacity, tunable porosity, and cost-effectiveness are some of the advantages of electrospun nanofibers in drug delivery.[1,14-17]

As an attempt to assess the advantages of these two classes of nanomaterials, this study developed a double-shelled hollow MSNs-embedded nanofiber (DSH-MSNs/PCL) system to achieve a sustained antibiotic release. For this purpose, the study explored the cefazolin (Cef) release profile and antibacterial activity of nanofibers against *Staphylococcus aureus* (*S. aureus*). The potential of nanofiber mats for human adipose-derived stem cells (hADSCs) differentiation into keratinocyte cells was also evaluated after 21 days.

## Materials and Methods

### *Materials*

Cetyltrimethylammonium bromide (CTAB), polycaprolactone (PCL), tetraethyl orthosilicate (TEOS), 3-(4,5-dimethyl-2-thiazolyl)-2,5-diphenyl tetrazolium bromide (MTT), hydrochloric acid, 3-aminopropyltriethoxysilane (APTES), and acetic acid were provided from Sigma-Aldrich [5]. Ammonia solution (32%), sodium carbonate ($Na_2CO_3$), ethanol (96%), and methanol (99.9%) were purchased from Merck (Germany). cDNA synthesis and RNA extraction kits were obtained from Parstous Co. (Mashhad, Iran). SYBR Green real-time-PCR Master Mix was provided from Ampliqon (Denmark). Fetal bovine serum (FBS), trypsin, penicillin, and streptomycin (P/S) were purchased from GIBCO (Grand Island, NY, USA). Dimethyl sulfoxide (DMSO) was supplied from Amresco (Solon, OH, USA). Lastly, the DMEM medium was purchased from Bio-Idea (Tehran, Iran).

### *Synthesis of DSH-MSNs*

DSH-MSNs were synthesized via previously established methods.[18] First, TEOS was hydrolyzed using the Stöber method to prepare monodisperse solid silica spheres. Briefly, a mixed solution containing 10 mL of water, 3.15 mL of ammonia solution (25%), and 74 mL of

ethanol was prepared to which TEOS (6 mL) was added. After 1 h, the white suspension was centrifuged at 12,000 rpm for 2 min and thoroughly rinsed with ethanol three times. The precipitation was dried at 60 °C for 6 h.
Later, 300 mg of the sample was dispersed in 60 mL of water and sonicated for 30 min. Subsequently, CTAB (450 mg), water (90 mL), ethanol (90 mL), and ammonia solution (1.65 mL) were added to the suspension and stirred for 30 min. 35 µL APTES and 750 µL TEOS were added and stirred for 6 h. Then, the sample was centrifuged and washed with water and ethanol. The sediment was dried at 60 °C for 6 h. Afterward, the sample was dispersed in water (60 mL), and 1.2 g of anhydrous $Na_2CO_3$ was added to the solution. The mixture was stirred at 50 °C for 10 h and subsequently centrifuged and washed. The sedimentation was dispersed in ethanol again. Lastly, 0.1 mL of HCl was added to the sample and stirred at 60 °C for 5 h to eliminate CTAB. DSH-MSNs were obtained after centrifuging, washing, and drying.

***Drug loading***

For drug loading into DSH-MSNs, different amounts of cefazolin (6, 9, 12, and 15 mg) were suspended in 1 mL of DSH-MSNs (3 mg/mL) aqueous suspension and stirred for 18-24 h at 25 °C. The Cef-loaded DSH-MSNs (Cef*DSH-MSNs) were then centrifuged for 2 minutes at 12,000 rpm and rinsed with water to remove free drug molecules. The sediment was dried in a desiccator.[19] The loading content of Cef was measured using the standard curve of the Cef solution. The following formulae were used to determine the drug loading content and loading efficiency:[19-21]

Drug loading content= (weight of the loaded drug in DSH-MSNs/ weight of drug and DSH-MSNs)×100% (Eq.1)

Drug loading efficiency= (weight of the loaded drug in DSH-MSNs/weight of feeding drug) ×100% (Eq. 2)

The amount of Cef in the supernatant was measured by spectrophotometry at 270 nm.

***Synthesis of nanofibers***

PCL solution (20%, viscosity: 27.8 cP) was prepared by dissolving PCL in acetic acid (90%) and stirring for 18-24 h at 25 °C. Subsequently, nanoparticles (DSH-MSNs and Cef*DSH-MSNs) and Cef were added to the PCL solution separately. In the next step, the prepared solutions were poured into a syringe (5 mL) with a needle tip (18G), and the fibers were collected on a grounded collector covered with aluminum foil. The optimal electrospinning parameters included a voltage of 14 kV, a 15 cm needle to collector distance, a flow rate of 1 mL/h, and a rotational speed of 200 rpm.

***Physicochemical characterization***

The structure of Cef*DSH-MSNs, DSH-MSNs, Cef, Cef*DSH-MSNs/PCL, Cef*PCL, and PCL were evaluated with an FT-IR spectrometer (IR prestige-21, Shimadzu Co., Japan) in the spectral range of 4000-400 $cm^{-1}$ using a potassium bromide disk (resolution of 4 $cm^{-1}$). Next, 5-6 mg of samples were mixed, triturated with 100 mg potassium bromide, and placed in a sample holder for the potassium bromide disk. The surface morphologies of the DSH-MSNs and nanofibers were observed by SEM (FEI Quanta 450 Field Emission Scanning Electron Microscope, USA). The particle size of DSH-MSNs was characterized by a Transmission Electron Microscope Test Instrument (Carl Zeiss-EM10C-100Kv, Germany).
The particle size distribution of DSH-MSNs dispersed in water was determined by DLS (Brookhaven, USA). A Zeta sizer Nano apparatus (Brookhaven, USA) was applied to measure the surface charge of the DSH-MSNs and Cef.

The water contact angle (WCA) of nanofibers was measured by a water contact angle analyzer (Veho discovery VMS-004 Deluxe, England). Moreover, water droplets (1 µL) were pipetted onto the surface of PCL nanofibers before and after loading of DSH-MSNs.

***Degradation Study***

Hydrolytic degradation of the nanofibers was conducted in PBS solution (pH = 7.4) for up to 4 weeks. The membranes were taken out from the PBS and characterized with SEM at week 4.

***Mechanical properties and tensile strength of nanofibers***

Electrospun nanofiber mats' mechanical properties and tensile strength play an essential role in tissue engineering. The mechanical properties of PCL nanofibers were evaluated before and after loading DSH-MSNs using a mechanical tensile testing device (Santam, STM-1, Iran). All nanofibers were cut in dimensions of 15 mm × 40 mm. The length of the nanofibers in the machine was 25 mm, and the tensile speed was 10 mm/min.

***The cefazolin release profile of nanofiber mats***

As a measure to determine the cefazolin release profile, 20 mg (three replicates) of the electrospun nanofiber mats (Cef*DSH-MSNs/PCL and Cef*PCL) were weighted and sterilized with UV light for 20 min. Twenty mg of nanofibers were immersed in 3 mL PBS at pH 7.4 in a bain-marie at 37 °C.[22] The released medium was replaced with a fresh medium (3 mL) after the defined time intervals. Eventually, the concentrations of Cef were measured by UV/V spectroscopy at 270 nm.

***Antibacterial assessment***

*Standard broth dilution method*

As a model for antibiotic drug, *S. aureus* (ATCC® 16,538™) was used to evaluate the antibacterial effects of Cef*DSH-MSNs/PCL, Cef*PCL, PCL, and DSH-MSNs/PCL. For quantitative analysis, 20 mg of the nanofiber mats were incubated in 5 mL of Luria broth (LB) medium containing *S. aureus* (OD: 0.3) at 37 °C for 18-24 h. Subsequently, 100 µL solution of each tube was diluted and cultured on an agar medium. The number of colonies was counted after incubating plates at 37 °C for 17 h. The bacterial suspension constituted the control group. All experiments were conducted in triplicate.

***Disc diffusion method***

Disc diffusion test was performed to determine the growth-suppressing action of Cef*DSH-MSNs/PCL, Cef*PCL, PCL, and DSH-MSNs/PCL. In this method, 0.5 McFarland sterile normal saline suspension was prepared from freshly growing *S. aureus* (ATCC® 16,538™) culture. The punched electrospun nanofiber discs (6 mm) were placed on LB agar medium with the bacteria suspension (0.5 McFarland standard) and incubated at 37 °C. A ruler was utilized to measure the inhibition zone in millimeters (mm). Three replicates were conducted under similar conditions for each sample.

***Cell culture***

*Cell viability assay*

The toxicity of PCL and DSH-MSNs/PCL was determined using MTT assay on hADSCs. Human adipose-derived stem cells were kindly gifted by Dr. Mohsen Khorashadizadeh from Birjand University of Medical Science.[23] For the MTT assay, $3\times10^4$ cells/well were seeded in 24-well plates, treated with sterile nanofiber mats after 24 h and incubated at 37 °C with 5%

$CO_2$ for 72 h. The medium was then substituted with 100 µL of MTT solution (1 mL fresh medium) and incubated at 37 °C for 4 h. For the formazan crystals formed by live cells to dissolve, the medium was removed entirely, and 500 µL of DMSO was added to each well plate. After 5 min, the absorbance was read on an ELISA plate reader at 570 nm.
The cell viability (%) was calculated as follow:
viable cells (%) = $\mathrm{abs}_{\mathrm{sample}} - \mathrm{abs}_{blank}/\mathrm{abs}_{\mathrm{control}} - \mathrm{abs}_{\mathrm{blank}} \times 100$ (Eq. 3).

***Cell seeding and differentiation of hADSCs into Keratinocytes***

PCL and DSH-MSNs/PCL nanofibers were cut (circular disks in 15 mm diameter) and placed in a laminar flow hood to sterilize using UV radiation so as to prepare nanofiber mats for cell seeding. Afterward, the nanofiber mats were washed to remove any residual solvent. The nanofibers were immersed in DMEM overnight to facilitate cell attachment on the nanofiber surfaces. Next, 200 µL of cell suspension (cell density: $2\times10^4$ cells/mL) were poured onto the surface of scaffolds and placed in an incubator for 4 h (5% $CO_2$ at 37 °C). After the cells were attached to the nanofiber mats, the additional medium was added, and incubation was resumed. The fresh medium was replaced every two days during the incubation period, and this process was continued for 21 days.

***Quantitative analysis of gene expression***

After 21 days, qRT-PCR was performed to assess the expressions of specific genes. Total RNA was extracted from cells using the Total RNA Extraction Kit (Parstous, Mashhad, Iran) as per the manufacturer's protocol. Complementary DNA was prepared using the RevertAid First-Strand cDNA Synthesis Kit (Parstous, Mashhad, Iran) following the manufacturer's instructions. For qRT-PCR, the amplification of the involucrin (IVL) and cytokeratin 18 (CK18) was performed using SYBR Green qRT-PCR Master Mix (A325402, Ampliqon, Denmark). Thermal cycling was carried out for 35 cycles of 30 s at 95 °C, 1 min at 60 °C for IVL and 58 °C for CK18, and 30 s at 72 °C. Primer sequences were as follows: IVL, forward: 5′ CAGCACTCCACCAAAGCCTC 3′ and reverse: 3′ GCTCCTGATGGGTATTGACTG 5′; CK18, forward: 5′ TCGCAAATACTGTGGACAATGC 3′ and reverse: 3′ GCAGTCGTGTGATATTGGTGT; and GAPDH, forward: 5′ TGGACTCCACGACGTACTCAG 3′ and reverse: 3′ CGGGAAGCTTGTCATCAATGGAA 5′. The qRT-PCR data were analyzed by the $2^{-\Delta\Delta ct}$ method and normalized to glyceraldehyde-3-phosphate dehydrogenase.

***Statistical Analysis***

All data were summarized as mean ± SD, and statistical analysis was performed by t-test (two-tailed) using GraphPad Prism (version 8.3.0) and REST (2009). A *P*-value of less than 0.05 was considered to be statistically significant.

**Results and Discussion**

***Characterization of DSH-MSNs***

DSH-MSNs were successfully synthesized by the Stöber method (Figure 1). DSH-MSNs had a round shape, an average particle size of approximately 400 nm, and a shell thickness of ~10 nm, as shown in SEM and TEM images (Figure 2a-f). The TEM image depicted a double-shelled structure, highly uniform size, and the shell thickness of nanoparticles (Figure 2f). The nanoparticles' zeta potential (pH=7.4) showed that DSH-MSNs were charged negatively (-17.31). The negative zeta potential of nanoparticles also revealed that the CTAB was removed from the structure.

In this study, the adsorption method was used for loading drugs into the pores of MSNs. Accordingly, DSH-MSNs were immersed in the concentrated cefazolin solution. After 24 h, the cefazolin molecules were absorbed on the pore walls. Drug-carrier interactions such as covalent bonding, electrostatic binding, hydrogen bonding, and van der Waals interactions facilitate the absorption of drug molecules in MSNs.[24,25] Moreover, Cef loading into DSH-MSNs was achieved by hydrogen bonding interactions between the OH of DSH-MSNs (silica) and Cef. The FT-IR spectrum of DSH-MSNs (Figure 2g) showed sharp bands at 3415, 2927, 2856, 1635, 1097, 962, 800, and 472 $cm^{-1}$.[18] The FT-IR spectrum of Cef (Figure 2h) displayed sharp bands at 3415, 3284, 3143, 3059, 2960, 2862, 1761, 1674, 1600, 1550, 1489, 1282, 1240,1184, 1101, and 1064 $cm^{-1}$.[26] The sharp peaks at 3415, 3284, and 1600 $cm^{-1}$ were related to the vibration of N-H stretching and the bending vibration of Cef.

The FT-IR spectrum of the Cef*DSH-MSNs (Figure 2i) indicated sharp bands at 3419, 3304, 3005, 2926, 2858, 1761, 1649, 1625, 1544, 1490, 1103, and 958 $cm^{-1}$ and broadband at 3600-2500 $cm^{-1}$. The peaks at 3419, 3304, and 1597 $cm^{-1}$ were related to N-H stretching and the bending vibration of Cef and DSH-MSNs' second amine at the Cef*DSH-MSNs, respectively. Besides, the peaks at 1103 and 958 $cm^{-1}$ were connected with the C-O stretching vibration of the Cef and DSH-MSNs, respectively. The FT-IR spectrum of the prepared Cef*DSH-MSNs indicated that the peak at 3005 $cm^{-1}$ was characteristic of C-H stretching vibration, and the peaks at 1625, 1544, and 1490 $cm^{-1}$ were related to C=C vinyl and aromatic stretching vibration of Cef. The peaks at 1761 and 1647 $cm^{-1}$ were also correlated with C=O from Cef. The changes in the peak positions were observed from 3415 to 3419, 1674 to 1649, and 1600 to 1544 $cm^{-1}$. These results confirm the presence of Cef and DSH-MSNs in the spectrum of Cef*DSH-MSNs. In addition, the results confirm the intermolecular hydrogen-bonding reaction between the OH of DSH-MSNs and Cef.

In this study, the Cef*DSH-MSNs were mixed with the PCL solution to synthesize the nanofibers. It should be noted that the acid pH of the solution has no negative impact on the stability of silica nanoparticles.[27] In this regard, Moghaddam et al. (2020) demonstrated that the degradation rate of MSNs increased in alkaline conditions.[28] Similarly, Ahmed and Day (1987) evaluated the stability of cefazolin in different pH levels, indicating a higher degradation of cefazolin in the alkaline pH.[29] The FT-IR spectrum of PCL nanofibers was employed to investigate PCL, Cef*PCL, and Cef*DSH-MSN/PCL structures and the intermolecular hydrogen-bonding reaction between PCL and Cef. The FT-IR spectrum of Cef*DSH-MSNs/PCL (Figure 3o) indicated sharp bands at 3342, 3040, 2927, 2860, 1728, 1670, 1587, 1456, 1292, 1238, 1182, 1045, 960, and 731 $cm^{-1}$. The broad peak at 2500-3500 $cm^{-1}$ region also corresponded to OH stretching vibration group of carboxylic acid from Cef. The sharp peaks at 3342 and 1587 $cm^{-1}$ were characteristic of N-H stretching vibration and the bending vibration of Cef at the Cef*DSH-MSNs/PCL.

The presence of the peak at 1728 $cm^{-1}$ was correlated with C=O from Cef and PCL, and the peaks at 3342 and 1587 $cm^{-1}$ were a feature of N-H stretching vibration and bending vibration of Cef, which can confirm the synthesis of Cef*DSH-MSNs/PCL nanofiber mats. Also, the FT-IR spectrum of Cef*DSH-MSNs/PCL showed prominent shifting of the peaks compared with those of PCL and Cef. The peaks at 1105, 880, 451 $cm^{-1}$ were linked with Si–O–Si and Si–O stretching vibrations of DSH-MSNs, confirming the synthesis of Cef*DSH-MSNs. The peak positions shifted from 3400 to 3342, 1730 and 1724 to 1728, and 1591 to 1587 $cm^{-1}$. These findings confirm the presence of PCL and Cef in the spectrum of Cef*DSH-MSNs/PCL and the synthesis of Cef*DSH-MSNs/PCL nanofiber mats.

WCA was calculated for PCL and DSH-MSNs/PCL nanofiber mats (Figure 4a-c). The hydrophobicity of pure PCL and DSH-MSNs/PCL nanofiber mats were 105 and 133 degrees,

respectively. Figure 4c showed that the hydrophobicity of PCL nanofiber mats significantly increased after the addition of DSH-MSNs. Previous research also indicates that MSNs-embedded electrospun nanofibers can increase the hydrophobicity of nanofibers.[30]
The degradability of PCL was evaluated after four weeks using FE-SEM (Figure 4d and 4e). After *in vitro* incubation in PBS, the diameter of PCL nanofibers increased, indicating that the swelling of nanofibers occurred during incubation.

***Mechanical properties and tensile strength of nanofibers***

Electrospun nanofiber mats' tensile strength and mechanical properties play an essential role in tissue engineering. The mechanical properties of PCL nanofibers were evaluated before and after loading DSH-MSNs using a mechanical tensile testing device (Santam, STM-1, Iran). All nanofibers were cut in dimensions of 15 mm × 40 mm. The length of the nanofibers in the machine was 25 mm, and the tensile speed was 10 mm/min.
Figure 5a and Table 1 present the typical stress-strain curves of the PCL and DSH-MSNs/PCL nanofiber mats. DSH-MSNs/PCL nanofibers have significantly higher mechanical properties than PCL ones. Indeed, when DSH-MSNs were added to PCL nanofibers, the nanofibers' thickness and size uniformity increased, leading to higher adhesion forces (cohesion), which is ultimately associated with enhanced mechanical properties. Furthermore, the high affinity between DSH-MSNs and PCL matrix resulted in better dispersion of DSH-MSNs in nanofibers, which may explain such reinforcement stress transitions.[31]
Gounani et al. and Ganesh et al. have demonstrated the increase in young's modulus of PCL mats after silica nanoparticles are added.[32,33] Similar to the case with PCL nanofibers, the mesoporous silica nanoparticles embedded into PLGA nanofibers revealed an increase in young's modulus and tensile strength_.[34] The similarity of the mechanical properties of scaffolds to those of the host tissue is one of the crucial goals of tissue engineering. Based on the values reported for tensile properties of different body tissues, the PCL and DSH-MSNs/PCL mats can serve as scaffolds in skin tissue engineering.[35]

**Table 1.** Tensile strength, young's modulus, and elongation at break of the PCL and DSH-MSNs/PCL nanofiber mats

| | Young's modulus (MPa) | Ultimate strength (MPa) | Elongation at break |
|---|---|---|---|
| **PCL** | 19.35±2.74 | 3.89±0.28 | 1.09±0.12 |
| **DSH-MSNs/PCL** | 20.26±1.69 | 8.02±0.41 | 0.45±0.7 |

***The drug loading properties of Cef*DSH-MSNs/PCL and Cef*PCL***

As Table 2 indicates, the loading content and loading efficiency of DSH-MSNs were 10.27–51.79% and 5.72–26.85%, respectively. DSH-MSNs and Cef were used in the ratio of 3:12 to synthesize nanofiber mats. Some attractive properties such as large surface area and high pore volume introduce MSNs as excellent materials for loading drugs. Furthermore, a perfect mesoporous structure and the tunable pore size of MSNs help better control drug loading and release kinetics.[36] Although MSNs have been broadly evaluated as drug delivery vehicles, the low drug-loading capacity remains the biggest challenge for these materials.[37] As a strategy to solve this problem, hollow MSNs with a large cavity inside each original MSN have been developed to enhance the loading capacity of drugs.[37] The high loading capacity of DSH-MSNs (51%) in this study indicates the practical application of DSH-MSNs as a drug delivery vehicle.

**Table 2.** Cef-loading content and loading efficiency of different concentrations

| DSH-MSNs | Cef | Drug loading content (w/w %) | Drug loading efficiency (%) |
|---|---|---|---|
| 3 mg | 6 mg | 10.27 | 5.72 |
| 3 mg | 9 mg | 27.41 | 12.58 |
| 3 mg | 12 mg | 51.79 | 26.85 |
| 3 mg | 15 mg | 31.99 | 9.41 |

***The drug release properties of Cef*DSH-MSNs/PCL and Cef*PCL nanofiber mats***

For the Cef release profile, the drug-loaded nanofibers were soaked in PBS (pH=7.4). Figure 5b illustrates the findings of the drug release profiles of Cef*DSH-MSNs/PCL and Cef*PCL nanofiber mats. The drug release curve of the samples showed that the release of Cef encapsulated in DSH-MSNs was slower than the Cef incorporated in PCL nanofibers. The drug release rate increased slowly after a few hours in the Cef*DSH-MSNs/PCL nanofiber mats, while the drug in the Cef*PCL nanofibers had a burst release. Multi-shelled hollow MSNs with high penetrating mesostructured shells sustain the drug release to a certain degree.[38] However, an initial burst release is typically observed in these drug delivery systems.[18] The incorporation of Cef*DSH-MSNs into PCL nanofibers revealed a more controlled release behavior. Drug release from pore DSH-MSNs and subsequently from nanofibers provide compelling evidence for the significantly slow release of Cef from Cef*DSH-MSNs/PCL nanofibers.[39] This mechanism can prevent the initial burst release of the drug and increase the local concentration of the drug over time.[40] Similarly, antibacterial tests confirmed a slow and controlled release from Cef*DSH-MSNs/PCL nanofiber mats. These preliminary results demonstrate the feasibility of using DSH-MSNs/PCL nanofibers for wound healing applications.

***Antibacterial activity of Cef*DSH-MSNs/PCL and Cef*PCL nanofiber mats in broth microdilution under standard in vitro conditions***

The antibacterial effects of PCL, DSH-MSNs/PCL, Cef*DSH-MSN/PCL, and Cef*PCL groups were determined via the standard broth dilution method. As Figure 6 depicts, Cef*DSH-MSN/PCL and Cef*PCL significantly decreased bacterial growth after 24 h. Cef*PCL showed more lethality than Cef*DSH-MSNs/PCL, consistent with experimental data from the drug release profile. However, both groups demonstrated a significant difference from the control group ($P < 0.05$) (Figure 6a and 6b). The potential antibacterial activities of PCL, DSH-MSNs/PCL, Cef*DSH-MSNs/PCL, and Cef*PCL nanofiber mats were also evaluated against *S. aureus* (ATCC® 16,538™) through the disc diffusion method. As shown in Figure 6c, Cef*DSH-MSNs/PCL and Cef*PCL nanofiber mats inhibited the growth of *S. aureus* with inhibition zones of 9 mm for Cef*DSH-MSNs/PCL and 38 mm for Cef*PCL. For PCL and DSH-MSNs/PCL, there was no significant difference in inhibition zones. Infection, a significant problem in burn wounds, can effectively delay healing.[41] Moreover, antibacterial resistance is one of the critical challenges for treating burn wounds. Although antibiotics significantly inhibit the growth of bacteria, high-dose antibiotic therapy may lead to toxic side effects in clinical practice.[42] On the other hand, bacterial adhesion to the bandage surface and, eventually, biofilm formation are challenges that limit the applicability of some bandages.[43]

***Cytotoxicity***

The hADSCs viability upon 72 h exposure to DSH-MSNs and PCL nanofibers was quantified using MTT assay to evaluate possible cytotoxicity of the synthesized nanoparticles and

nanofibers (Figure 7a). The nanoengineered membranes showed no toxicity to hADSCs, and cells were well grown on the surface of nanofibers without changes in morphology ($P > 0.05$). In agreement with our findings, numerous experiments investigating the cytotoxicity of silica nanoparticles in different cell lines have reported that silica nanoparticles have no toxic effects.[44-48]

***Gene expression analysis***

To determine whether PCL and DSH-MSNs/PCL can stimulate the differentiation of hADSCs toward keratinocytes, we evaluated the expression of IVL and CK18 by qRT-PCR. As shown in Figure 7b, there was a significant increase in the mRNA expression level of IVL in the PCL and DSH-MSNs/PCL nanofiber mats compared with the control group after 21 days ($P < 0.05$). As against the PCL group, the IVL expression was significantly high in the DSH-MSNs/PCL group ($P < 0.05$). However, the qRT-PCR data in Figure 7c exhibited a significant reduction in the mRNA expression level of CK18 in the PCL and DSH-MSNs/PCL groups after 21 days ($P > 0.05$). In this regard, Yang et al. (2020) also demonstrated that the expression of CK18 in the absence of an induction medium was negative.[44,49]

Epithelialization is a vital stage in wound healing, and keratinocytes play a crucial role in promoting re-epithelialization.[50] Poor quality and insufficient quantity of keratinocytes in unfavorable conditions such as severe burns may impair wound healing.[51] Differentiating hASCs toward keratinocytes can be a good solution for promoting burn wound healing. Few researchers have demonstrated the capacity of hADSCs in epidermal differentiation using nanoparticles and scaffolds.[52,53] According to previous studies, cells often need an induction medium for differentiation.[54] In our study, the differentiation effect of synthesized 3D scaffolds on hADSCs into keratinocytes was assessed without using an induction medium.

The results of qRT-PCR revealed that the IVL expression level in the presence of scaffolds (DSH*MSNs/PCL, PCL) was significantly increased. Notably, the DSH-MSNs/PCL demonstrated a substantially influential role in IVL modulation compared to PCL nanofiber mats. In this regard, several studies have shown that nanoparticles can easily insert into cell membranes, locate in the cytoplasm, affect cellular signaling pathways, and induce differentiation by virtue of their small size.[54] Based on Wei et al.'s (2017) findings, silica nanoparticles' unique biological and mechanical properties are another possible contributor to stem cell differentiation.[54] Nanofiber scaffolds also facilitate the differentiation of ASCs into epidermal cells by mimicking the structure and function of ECM.[52] Alongside this, Ganesh et al. (2012) demonstrated, for the first time, that electrospun MSNs/PCL nanofiber mats could induce differentiation of hMSCs to osteogenic cells.[32] It should be noted that three-dimensional culture provides the biochemical aspects of cell-cell communication, signaling mechanisms, plasticity, cell proliferation, and migration to induce differentiation.[55,56] Besides, scaffolds provide conditions for cell growth and differentiation into keratinocytes by mimicking the extracellular matrix and creating a 3D environment.[57]

The large cavity of DSH-MSNs not only increases the loading capacity but also prolongs the release profile of the drug. The differentiation effect of DSH-MSNs and PCL nanofibers on hADSCs into keratinocytes is another reason that considers DSH-MSNs as a good strategy for promoting wound healing. Our findings are promising and should be explored with other tests. Future work should focus on loading the two drugs, evaluating the long-term toxicity of DSH-MSNs, and assessing their impact on wound healing in animal models.

## Conclusion

This study has developed a composite nanofibrous material for controlled and sustained drug release. The incorporation of Cef*DSH-MSNs into PCL nanofibers significantly reduced the burst release of the cefazolin and led to a sustained drug release. The drug-loaded nanofiber mats were effective against *S. aureus* and significantly inhibited their growth. The DSH-MSNs/PCL also significantly stimulated the differentiation of human adipose stem cells to keratinocytes. Hence, the Cef*DSH-MSNs/PCL nanofiber mats demonstrated their potential in drug delivery and regenerative medicine.

**Acknowledgments**
The office of Vice-Chancellor for Research and Technology, Birjand University of Medical Sciences, supported his research project (grant number: Ir.bums.456090).

**Conflict of interests**
There is no conflict of interest to declare.

**References**
1. Alemzadeh E, Oryan A. Effectiveness of a Crocus sativus extract on burn wounds in rats. *Planta Med.* 2018;84(16):1191-200. doi: 10.055/a-0631-3620.
2. Alemzadeh E, Oryan A, Mohammadi AA. Hyaluronic acid hydrogel loaded by adipose stem cells enhances wound healing by modulating IL- 1β, TGF- β1, and bFGF in burn wound model in rat. *J Biomed Mater Res Part B Appl Biomater* 2020;108(2):555-67. doi: 10.1002/jbm.b.34411
3. Percival SL, McCarty SM, Lipsky B. Biofilms and wounds: an overview of the evidence. *Adv Wound Care* 2015;4(7):373-81. doi: 10.1089/wound.2014.0557.
4. Li B, Webster TJ. Bacteria antibiotic resistance: New challenges and opportunities for implant- associated orthopedic infections. *J Orthop Res* 2018;36(1):22-32. doi: 10.1002/jor.23656
5. Patra JK, Das G, Fraceto LF, Campos EVR, Rodriguez-Torres MdP, Acosta-Torres LS, et al. Nano based drug delivery systems: recent developments and future prospects. *J Nanobiotechnology* 2018;16(1):1-33. doi: 10.1186/s12951-018-0392-8.
6. Safari J, Zarnegar Z. Advanced drug delivery systems: Nanotechnology of health design A review. *J Saudi Chem Soc* 2014;18(2):85-99. doi: 10.1016/j.jscs.2012.12.009
7. Suri SS, Fenniri H, Singh B. Nanotechnology-based drug delivery systems. *J Occup Med Toxicol* 2007;2(1):1-6. doi: 10.1186/745-6673-2-16
8. Sharma M, Sharma R, Jain DK. Nanotechnology based approaches for enhancing oral bioavailability of poorly water soluble antihypertensive drugs. *Scientifica.* 2016;2016. doi: 10.1155/2016/8525679.
9. Tiwari G, Tiwari R, Sriwastawa B, Bhati L, Pandey S, Pandey P, et al. Drug delivery systems: An updated review. *Int J Pharm Investig* 2012;2(1):2. doi: 10.4103/2230-973X.96920
10. Popat A, Hartono SB, Stahr F, Liu J, Qiao SZ, Lu GQM. Mesoporous silica nanoparticles for bioadsorption, enzyme immobilisation, and delivery carriers. *Nanoscale.* 2011;3(7):2801-18. doi: 10.1039/C1NR10224A.
11. Vallet-Regí M, Colilla M, Izquierdo-Barba I, Manzano M. Mesoporous silica nanoparticles for drug delivery: Current insights. *Molecules.* 2018;23(1):47. doi: 10.3390/molecules23010047.

12. Jafari A, Amirsadeghi A, Hassanajili S, Azarpira N. Bioactive antibacterial bilayer PCL/gelatin nanofibrous scaffold promotes full-thickness wound healing. *Int J Pharm* 2020;583:119413. doi: 10.1016/j.ijpharm.2020.
13. Saveh-Shemshaki N, Nair LS, Laurencin CT. Nanofiber-based matrices for rotator cuff regenerative engineering. *Acta Biomater* 2019;94:64-81. doi: 10.1016/j.actbio.2019.05.041.
14. Qiu K, He C, Feng W, Wang W, Zhou X, Yin Z, et al. Doxorubicin-loaded electrospun poly (L-lactic acid)/mesoporous silica nanoparticles composite nanofibers for potential postsurgical cancer treatment. *J Mater Chem B* 2013;1(36):4601-11. doi: 10.1039/C3TB20636J.
15. Shahriar S, Mondal J, Hasan MN, Revuri V, Lee DY, Lee Y-K. Electrospinning nanofibers for therapeutics delivery. *Nanomaterials.* 2019;9(4):532. doi: 10.3390/nano9040532.
16. Torres-Martínez EJ, Cornejo Bravo JM, Serrano Medina A, Pérez González GL, Villarreal Gómez LJ. A summary of electrospun nanofibers as drug delivery system: Drugs loaded and biopolymers used as matrices. *Curr Drug Deliv* 2018;15(10):1360-74. doi: 10.2174/1567201815666180723114326
17. Zhang Y, Chang M, Bao F, Xing M, Wang E, Xu Q, et al. Multifunctional Zn doped hollow mesoporous silica/polycaprolactone electrospun membranes with enhanced hair follicle regeneration and antibacterial activity for wound healing. *Nanoscale.* 2019;11(13):6315-33. doi: 10.1039/C8NR09818B.
18. Cao L, Zhang H, Zhou Z, Xu C, Shan Y, Lin Y, et al. Fluorophore-free luminescent double-shelled hollow mesoporous silica nanoparticles as pesticide delivery vehicles. *Nanoscale.* 2018;10(43):20354-65. doi: 10.1039/c8nr04626c.
19. Hanafi-Bojd MY, Jaafari MR, Ramezanian N, Xue M, Amin M, Shahtahmassebi N, et al. Surface functionalized mesoporous silica nanoparticles as an effective carrier for epirubicin delivery to cancer cells. *Eur J Pharm Biopharm* 2015;89:248-58. doi: 10.1016/j.ejpb.2014.12.009
20. Gao F, Li L, Zhang H, Yang W, Chen H, Zhou J, et al. Deoxycholic acid modified-carboxymethyl curdlan conjugate as a novel carrier of epirubicin: in vitro and in vivo studies. *Int J Pharm* 2010;392(1-2):254-60. doi: 10.1016/j.ijpharm.2010.03.044
21. Hanafi-Bojd MY, Ansari L, Mosaffa F, Malaekeh-Nikouei B. The effect of mesoporous silica nanoparticles loaded with epirubicin on drug-resistant cancer cells. *Nanomed J* 2017;4(3):135-41. doi: 10.22038/nmj.2017.8954
22. Tort S, Demiröz FT, Yıldız S, Acartürk F. Effects of UV exposure time on nanofiber wound dressing properties during sterilization. *J Pharm Innov* 2020;15(3):325-32. doi: 10.1007/s12247-019-09383-7
23. Khorashadizadeh M, Soleimani M, Khanahmad H, Fallah A, Naderi M, Khorramizadeh M. Bypassing the need for pre-sensitization of cancer cells for anticancer TRAIL therapy with secretion of novel cell penetrable form of Smac from hA-MSCs as cellular delivery vehicle. *Tumor Biol* 2015;36(6):4213-21. doi: 10.1007/s13277-015-3058-2
24. Li Z, Zhang Y, Feng N. Mesoporous silica nanoparticles: Synthesis, classification, drug loading, pharmacokinetics, biocompatibility, and application in drug delivery. *Expert Opin Drug Deliv* 2019;16(3):219-37. doi: 10.1080/17425247.2019.1575806.
25. Trzeciak K, Chotera-Ouda A, Bak-Sypien II, Potrzebowski MJ. Mesoporous Silica Particles as Drug Delivery Systems—The State of the Art in Loading Methods and the Recent Progress in Analytical Techniques for Monitoring These Processes. *Pharmaceutics.* 2021;13(7):950. doi: 10.3390/pharmaceutics13070950

26. Rechelo BS, Kogawa AC, Salgado HRN. Quantitative analysis of cefazolin sodium in lyophilized powder by infrared spectrophotometry: Green, low cost, fast and effective. *Spectrochim Acta A Mol Biomol Spectrosc* 2019;208:157-61. doi: 10.1016/j.saa.2018.09.058
27. Rastegari E, Hsiao Y-J, Lai W-Y, Lai Y-H, Yang T-C, Chen S-J, et al. An update on mesoporous silica nanoparticle applications in nanomedicine. *Pharmaceutics.* 2021;13(7):1067. doi: 10.3390/pharmaceutics13071067.
28. Moghaddam SPH, Mohammadpour R, Ghandehari H. In vitro and in vivo evaluation of degradation, toxicity, biodistribution, and clearance of silica nanoparticles as a function of size, porosity, density, and composition. *J Control Release* 2019;311:1-15. doi: 0.1016/j.jconrel.2019.08.028.
29. Ahmed I, Day P. Stability of cefazolin sodium in various artificial tear solutions and aqueous vehicles. *Am J Hosp Pharm* 1987;44(10):2287-90. doi: 10.1093/ajhp/44.10.2287
30. Contreras-Cáceres R, Cabeza L, Perazzoli G, Díaz A, López-Romero JM, Melguizo C, et al. Electrospun nanofibers: Recent applications in drug delivery and cancer therapy. *Nanomaterials.* 2019;9(4):656. doi: 10.3390/nano9040656.
31. Eivazzadeh-Keihan R, Chenab KK, Taheri-Ledari R, Mosafer J, Hashemi SM, Mokhtarzadeh A, et al. Recent advances in the application of mesoporous silica-based nanomaterials for bone tissue engineering. *Mater Sci Eng* 2020;107:110267. doi: 10.1016/j.msec.2019. .
32. Ganesh N, Jayakumar R, Koyakutty M, Mony U, Nair SV. Embedded silica nanoparticles in poly (caprolactone) nanofibrous scaffolds enhanced osteogenic potential for bone tissue engineering. *Tissue Eng Part A* 2012;18(17-18):1867-81. doi: 10.089/ten.tea.2012.0167
33. Gounani Z, Pourianejad S, Asadollahi MA, Meyer RL, Rosenholm JM, Arpanaei A. Polycaprolactone-gelatin nanofibers incorporated with dual antibiotic-loaded carboxyl-modified silica nanoparticles. *J Mater Sci* 2020;55(36):17134-50. doi: 10.1007/s0853-020-05253-7.
34. Mehrasa M, Asadollahi MA, Nasri-Nasrabadi B, Ghaedi K, Salehi H, Dolatshahi-Pirouz A, et al. Incorporation of mesoporous silica nanoparticles into random electrospun PLGA and PLGA/gelatin nanofibrous scaffolds enhances mechanical and cell proliferation properties. *Mater Sci Eng C* 2016;66:25-32. doi: 10.1016/j.msec.2016.04.031.
35. Goudarzi ZM, Behzad T, Ghasemi-Mobarakeh L, Kharaziha M, Enayati MS. Structural and mechanical properties of fibrous poly (caprolactone)/gelatin nanocomposite incorporated with cellulose nanofibers. *Polym Bull* 2020;77(2):717-40. doi: 10.1007/s00289-019-2756-5.
36. Wang Y, Zhao Q, Han N, Bai L, Li J, Liu J, et al. Mesoporous silica nanoparticles in drug delivery and biomedical applications. *Nanomedicine.* 2015;11(2):313-27. doi: 10.1016/j.nano.2014.09.014
37. Bharti C, Nagaich U, Pal AK, Gulati N. Mesoporous silica nanoparticles in target drug delivery system: A review. *Int J Pharm Investig* 2015;5(3):124. doi: 10.4103/2230-973X.160844
38. Li Y, Shi J. Hollow- structured mesoporous materials: chemical synthesis, functionalization and applications. *Adv Mater* 2014;26(20):3176-205. doi: 10.1002/adma.201305319.
39. Xu C, Yu M, Noonan O, Zhang J, Song H, Zhang H, et al. Core- Cone Structured Monodispersed Mesoporous Silica Nanoparticles with Ultra- large Cavity for Protein Delivery. *Small.* 2015;11(44):5949-55. doi: 10.1002/smll.201501449

40. Chen K, Nikam SP, Zander ZK, Hsu Y-H, Dreger NZ, Cakmak M, et al. Continuous fabrication of antimicrobial nanofiber mats using post-electrospinning functionalization for roll-to-roll scale-up. *ACS Appl Polym Mater* 2020;2(2):304-16. doi: 10.1021/acsapm.9b00798
41. Church D, Elsayed S, Reid O, Winston B, Lindsay R. Burn wound infections. *Clin Microbiol Rev* 2006;19(2):403-34. doi: 10.1128/CMR.19.2.403-434.2006.
42. Rios AC, Moutinho CG, Pinto FC, Del Fiol FS, Jozala A, Chaud MV, et al. Alternatives to overcoming bacterial resistances: state-of-the-art. *Microbiol Res* 2016;191:51-80. doi: 10.1016/j.micres.2016.04.008.
43. Li X, Wu B, Chen H, Nan K, Jin Y, Sun L, et al. Recent developments in smart antibacterial surfaces to inhibit biofilm formation and bacterial infections. *J Mater Chem B* 2018;6(26):4274-92. doi: 10.1039/C8TB01245H.
44. Ema M, Kobayashi N, Naya M, Hanai S, Nakanishi J. Reproductive and developmental toxicity studies of manufactured nanomaterials. *Reprod Toxicol* 2010;30(3):343-52. doi: 10.1016/j.reprotox.2010.06.002.
45. Eom H-J, Choi J. Oxidative stress of silica nanoparticles in human bronchial epithelial cell, Beas-2B. *Toxicol In Vitro* 2009;23(7):1326-32. doi: 10.016/j.tiv.2009.07.010
46. Ha S-W, Sikorski JA, Weitzmann MN, Beck Jr GR. Bio-active engineered 50 nm silica nanoparticles with bone anabolic activity: therapeutic index, effective concentration, and cytotoxicity profile in vitro. *Toxicol In Vitro* 2014;28(3):354-64. doi: 10.1016/j.tiv.2013.12.001
47. Kim I-Y, Joachim E, Choi H, Kim K. Toxicity of silica nanoparticles depends on size, dose, and cell type. *Nanomedicine* 2015;11(6):1407-16. doi: 10.016/j.nano.2015.03.004
48. Marquis BJ, Love SA, Braun KL, Haynes CL. Analytical methods to assess nanoparticle toxicity. *Analyst.* 2009;134(3):425-39. doi: 10.1039/b818082b.
49. Yang F, Zhang W-L, Chen S-Q, Sun H-J, Lu J, Xiao X-F, et al. Differentiation of human adipose-derived stem cells into endometrial epithelial cells. *Reprod Dev Med* 2020;4(3):137. doi: 10.4103/2096-924.296547
50. Pastar I, Stojadinovic O, Yin NC, Ramirez H, Nusbaum AG, Sawaya A, et al. Epithelialization in wound healing: a comprehensive review. *Adv Wound Care* 2014;3(7):445-64.
51. Mishra PJ, Mishra PJ, Banerjee D. Keratinocyte induced differentiation of mesenchymal stem cells into dermal myofibroblasts: a role in effective wound healing. *Int J Transl Sci* 2016;2016(1):5. doi: 10.13052/ijts2246-8765.2016.002.
52. Li M, Ma J, Gao Y, Dong M, Zheng Z, Li Y, et al. Epithelial differentiation of human adipose-derived stem cells (hASCs) undergoing three-dimensional (3D) cultivation with collagen sponge scaffold (CSS) via an indirect co-culture strategy. *Stem Cell Res Ther* 2020;11(1):1-16. doi: 0.1186/s13287-020-01645-3
53. Lotfi M, Naderi- Meshkin H, Mahdipour E, Mafinezhad A, Bagherzadeh R, Sadeghnia HR, et al. Adipose tissue- derived mesenchymal stem cells and keratinocytes co- culture on gelatin/chitosan/β- glycerol phosphate nanoscaffold in skin regeneration. *Cell Biol Int* 2019;43(12):1365-78. doi: 10.002/cbin.11119
54. Wei M, Li S, Le W. Nanomaterials modulate stem cell differentiation: biological interaction and underlying mechanisms. *J Nanobiotechnology* 2017;15(1):1-13. doi: 0.1186/s12951-017-0310-5
55. Badekila AK, Kini S, Jaiswal AK. Fabrication techniques of biomimetic scaffolds in three-dimensional cell culture: A review. *J Cell Physiol* 2021;236(2):741-62. doi: 10.1002/jcp.29935

56. Patil S, Paul S. A comprehensive review on the role of various materials in the osteogenic differentiation of mesenchymal stem cells with a special focus on the association of heat shock proteins and nanoparticles. *Cells Tissues Organs.* 2014;199(2-3):81-102 doi: 10.1159/000362226
57. Shokrgozar MA, Fattahi M, Bonakdar S, Kashani IR, Majidi M, Haghighipour N, et al. Healing potential of mesenchymal stem cells cultured on a collagen-based scaffold for skin regeneration. *Iran Biomed J* 2012;16(2):68. doi: 10.6091/ibj.1053.2012

**Figure legends**

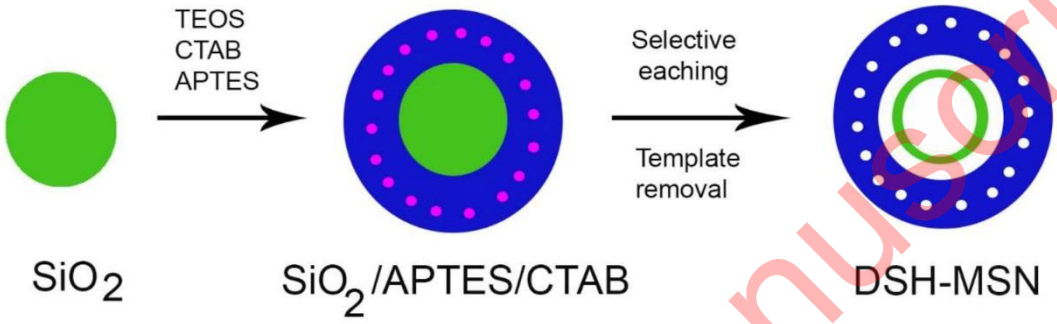


**Figure 1.** Schematic illustration of the preparation of DSH-MSNs.

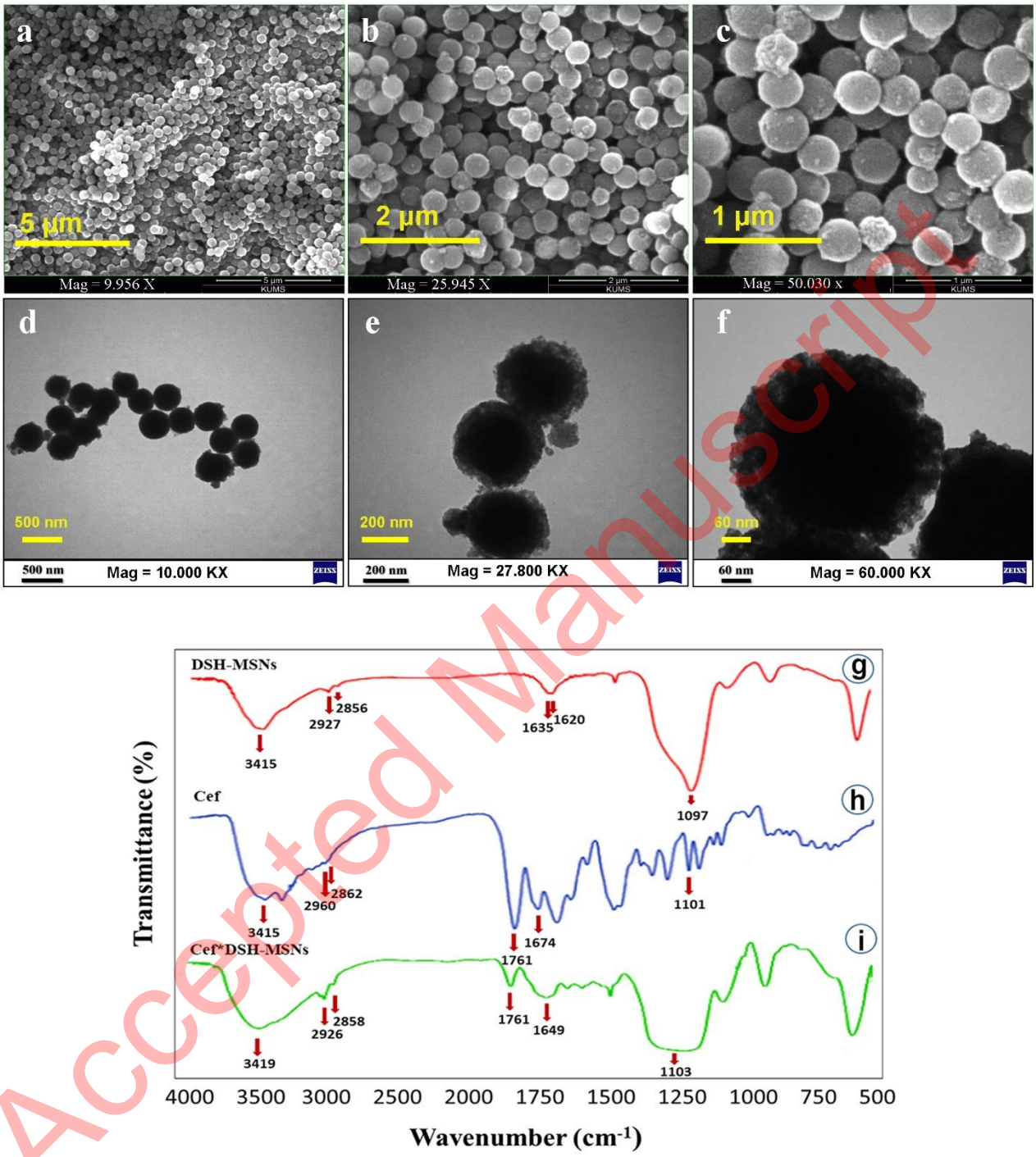


**Figure 2.** SEM (**a, b, c**) **(HV: 30.00 KV, spot: 3.5, WD: 10.3 mm)** and TEM (**d, e, f**) images of DSH-MSNs. Scale bars: (**a**) 5.0 µm; (**b**) 2.0 µm; (**c**) 1.0 µm; (**d**) 500 nm; (**e**) 200 nm; (**f**) 60 nm. FT-IR spectra of DSH-MSNs, Cef, and Cef*DSH-MSNs (**g-i**).

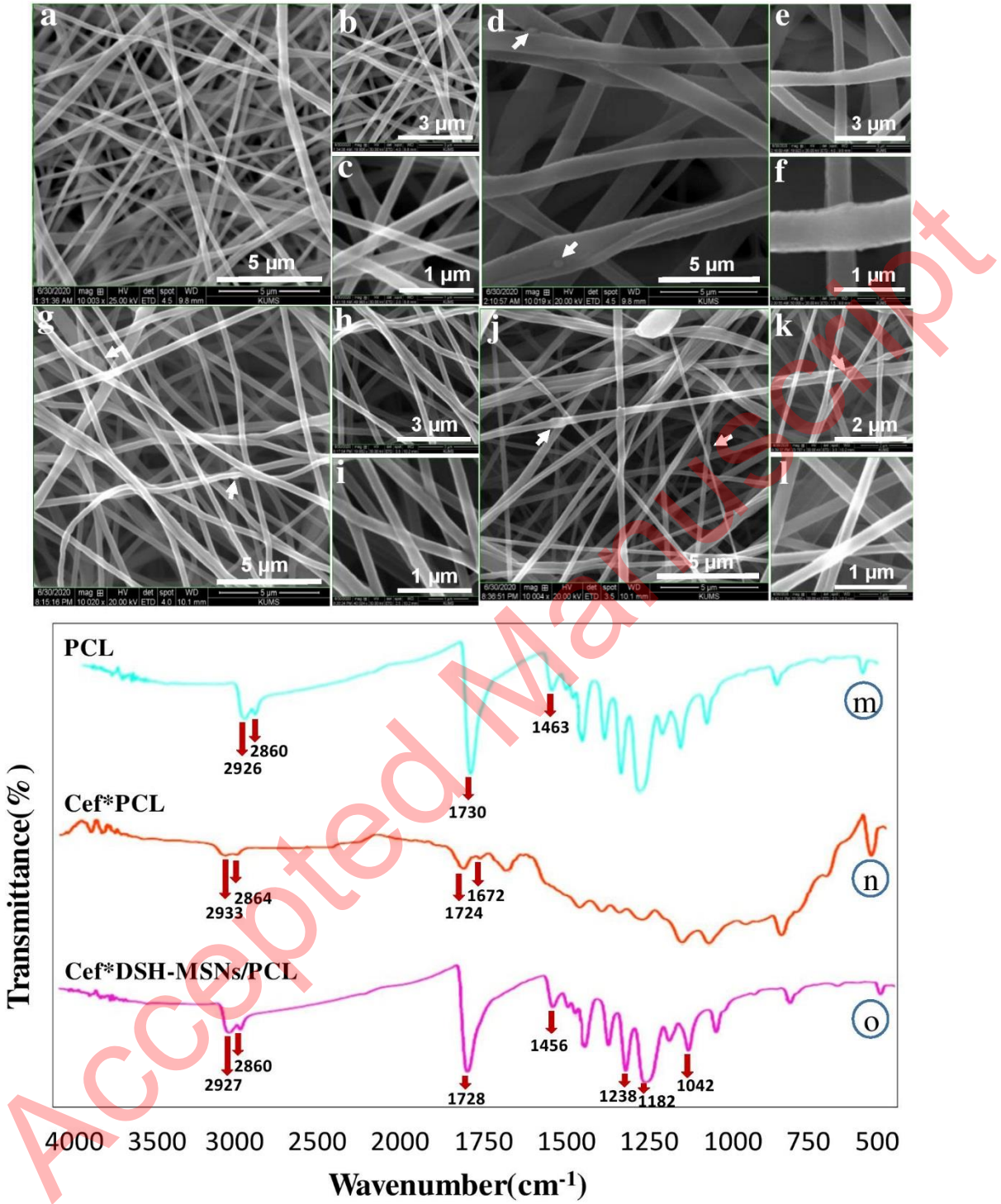


**Figure 3.** SEM images of PCL nanofibers. PCL (**a, b, c**), Cef*PCL (**d, e, f**), DSH-MSNs/PCL (**g, h, i**), and Cef*DSH-MSNs/PCL (**j, k, l**). Scale bars: (**a, d, g, j**) 5.0 µm; (**b, e, h**) 3.0 µm; (**k**) 2.0 µm; (**c, f, i, l**) 1.0 µm. FT-IR spectra of Cef*DSH-MSNs/PCL, Cef*PCL, and PCL (**m-o**).

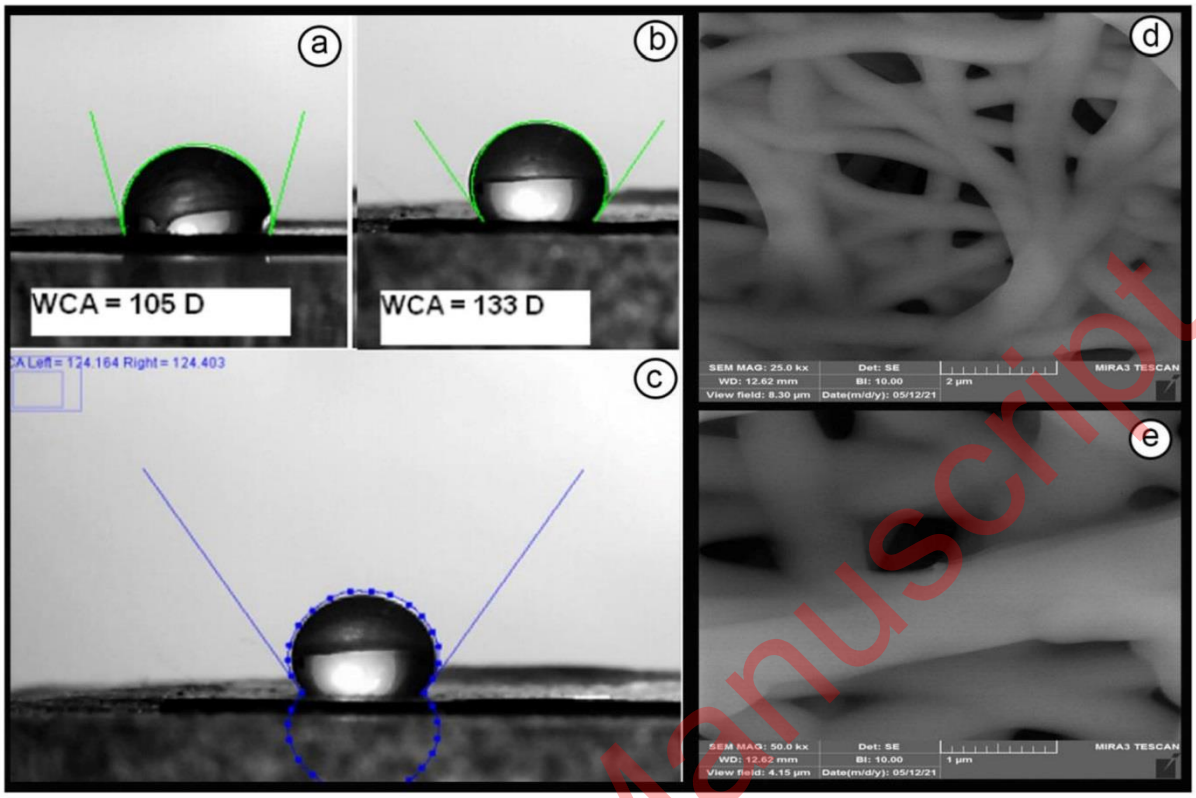


**Figure 4**. Water contact angle (**a**) Water drop on PCL nanofiber mats with 105 degrees (**b**) Water drop on DSH-MSNs/PCL nanofiber mats with 133 degrees (**c**) A water drop on the DSH-MSNs/PCL nanofiber mat surface showing contact angles of reflection below. (Note: water contact angle larger than 90 degrees, is considered hydrophobic). (**d, e**) FE-SEM images of *in vitro* degradation of electrospun PCL in PBS (pH=7.4). Scale bars: (**d**) 2 µm; (**e**) 1 µm.

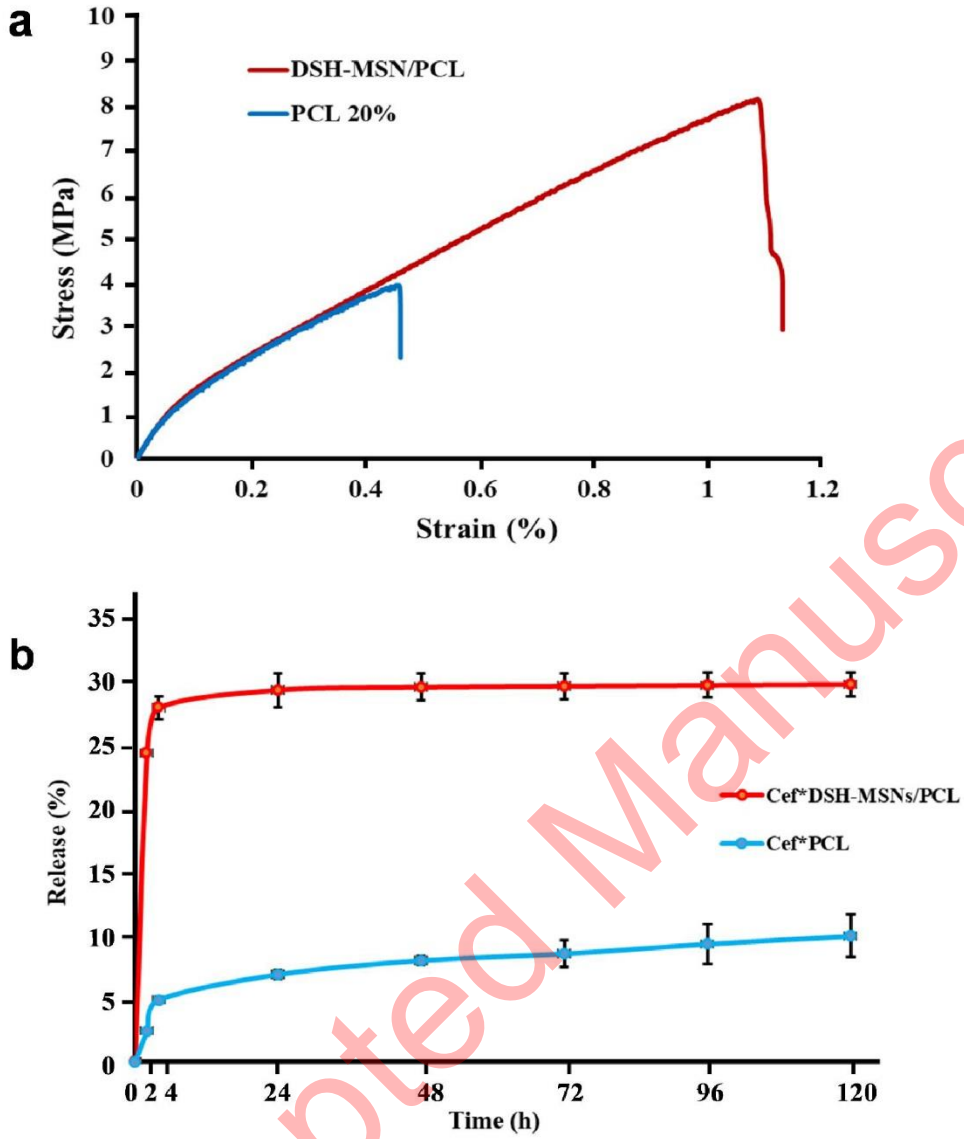


**Figure 5.** (**a**) Stress-strain curves of the PCL and DSH-MSNs/PCL nanofiber mats. (**b**) Release kinetics of cefazolin from Cef*DSH-MSNs/PCL and Cef*PCL nanofiber mats in phosphate buffer solution (PBS, pH=7.4) (mean ± SD, n=3).

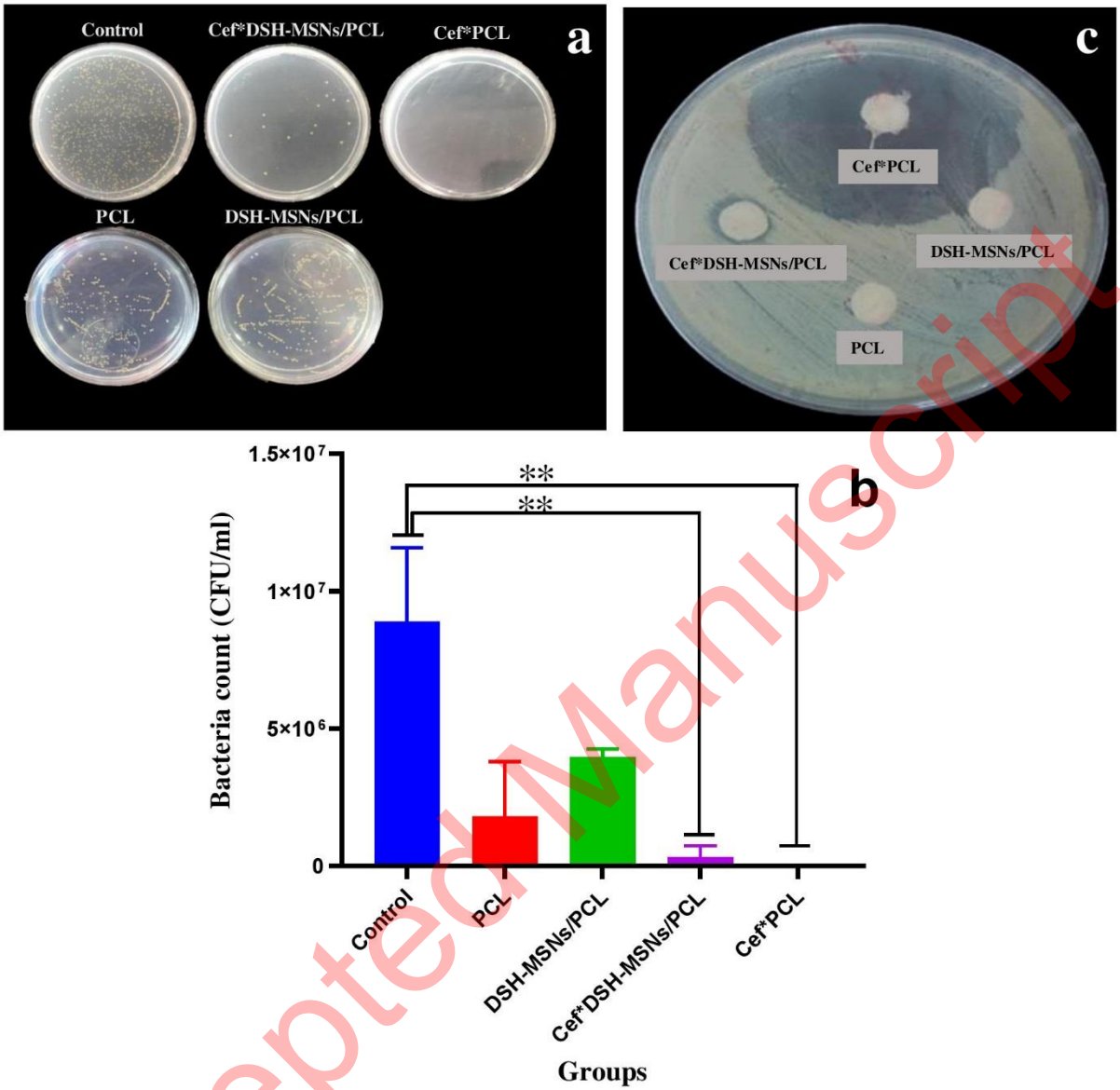


**Figure 6**. (**a, b**) Efficacy of Cef*DSH-MSNs/PCL, Cef*PCL against *S. aureus* (mean ± SD, n=3). (Note: * indicates Cef*DSH-MSNs/PCL, Cef*PCL significantly different to the other groups. ($P < 0.05$ *, $P < 0.01$ **). (**c**) *In vitro* antibacterial activity of Cef*DSH-MSNs/PCL, Cef*PCL against *S. aureus* (ATCC®16,538™). For PCL and DSH-MSNs/PCL there was no significant difference in the zone of inhibition.

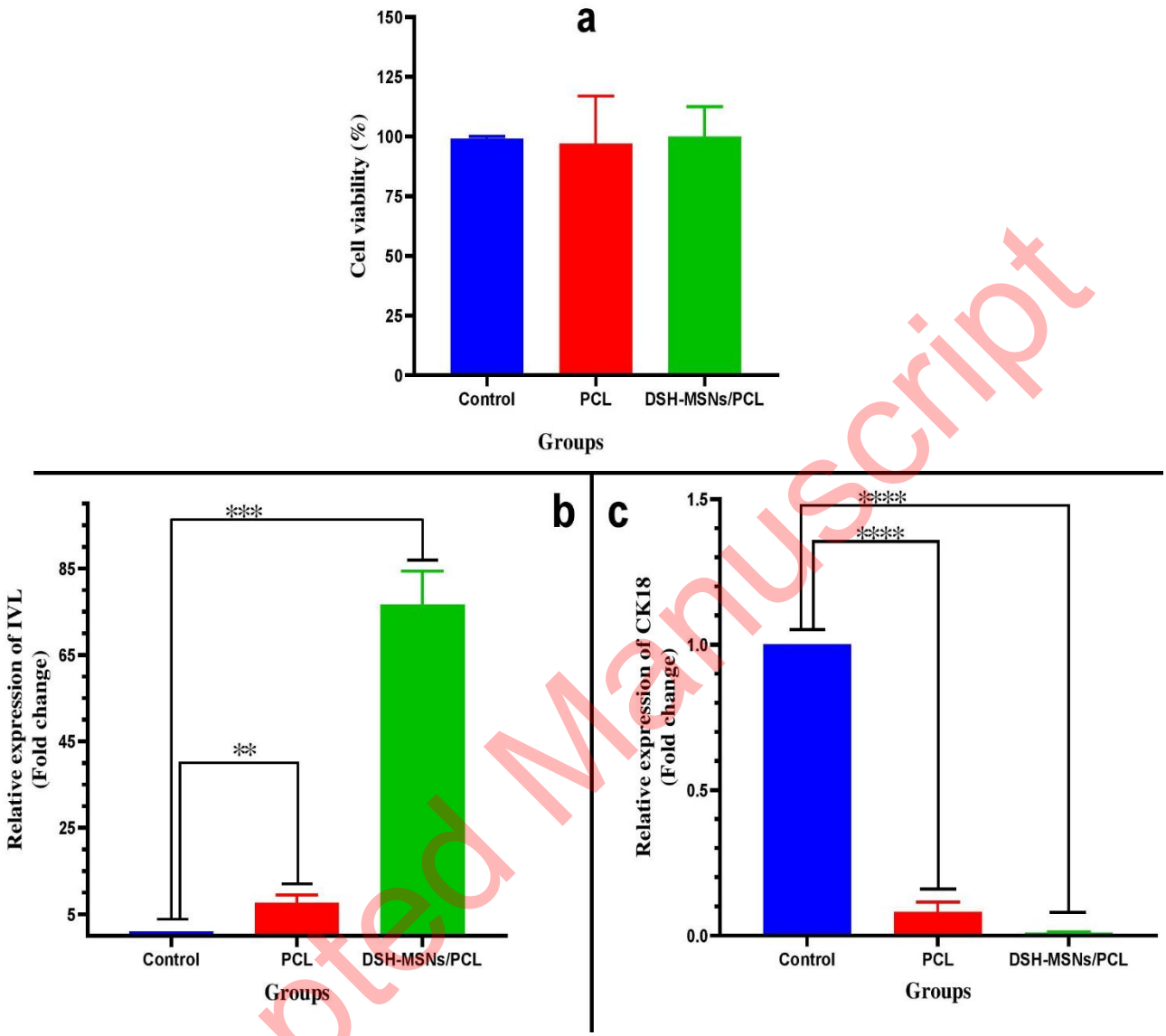


**Figure 7.** (**a**) Cell viability of hADSCs grown on PCL and DSH-MSNs/PCL ($P < 0.05$). Values are expressed as mean ± SD Modulation of IVL and CK18 profile by PCL and DSH-MSNs/PCL nanofiber mats: The mRNA levels of (**b**) Involucrin, (**c**) Cytokeratin18 at 21 days post-culturing, as determined by quantitative real-time PCR (Note: * indicates DSH-MSNs/PCL, PCL significantly different) ($P < 0.05$ *, $P < 0.01$ **, $P < 0.001$ ***, $P < 0.0001$ ****).